Photoinduced electron transfer in mechanically interlocked suit[3]ane systems

A. J. Stasyuk,*[a,b] O. A. Stasyuk,[a] M. Solà*[a] and A. A. Voityuk*[a,c]

a. Institut de Química Computacional and Departament de Química, Universitat de Girona, C/ Maria Aurèlia Capmany 69, 17003 Girona, Spain.

b. Faculty of Chemistry, University of Warsaw, Pasteura 1, 02-093 Warsaw, Poland

c. Institució Catalana de Recerca i Estudis Avancats (ICREA), 08010 Barcelona, Spain.

Abstract

Suitanes, a new class of two-component mechanically interlocked systems, have recently been developed. In this work, we report a detailed study of photoinduced electron transfer processes in suit[3]anes consisting of a 3-fold symmetric pyridinium-based (**$HC^{6+}\cdot 6PF_6^-$**) cage and substituted benzotrithiophenes, as well as other polycyclic aromatic guests. Analysis of electronic properties of the complexes shows that electron transfer is favorable for complexes of **$HC^{6+}\cdot 6PF_6^-$** with strong donors, such as thiatruxene, benzotrithiophenes, and benzotrifuran. The photoinduced electron transfer for these complexes occurs on the picosecond time scale. On the contrary, electron transfer does not occur in complexes **$HC^{6+}\cdot 6PF_6^-$** with benzotristiazole and benzotrisoxazole. Our results open perspectives for the future design of mechanically interlocked systems for application in photovoltaic devices.

Introduction

Mechanically interlocked molecules (MIMs) attract significant attention of scientists over the past few decades due to their unusual architecture.[1-3] The concept of mechanical bonding is an entanglement of two or more parts, which cannot be separated without breaking or substantial distorting chemical bonds between atoms of one of the fragments.[4,5] Structures of this type were first revealed to the world in 1960, when Wasserman synthetized a molecule, consisting of two interlocked rings, which was named a catenane.[6] The fact that the parts of MIMs do not directly connect to each other but cannot be separated without breaking the bond provides a new type of isomerism – topological isomerism. The concept of topological isomers of cyclic molecules was introduced by Frisch and Wasserman in 1961.[7] Topoisomers are chemically distinct structures that have the same number and type of atoms, which are linked to each other in the same way and characterized by identical stereochemical bond connectivity, but differ in topologies.[8-10] For a long time, architectures of MIMs were represented by catenanes,[11-14] rotaxanes,[14-17] molecular knots,[18,19] and their derivatives.[20-24] Only several years ago, a new type of MIMs that do not possess interlocked rings or dumbbell shaped molecule threaded through a macroring was introduced. Suitanes – a class of MIMs, which consist of two separate components — contains a body with two or more rigid limbs protruding outwards and a close-fitting, all-in-one suit.[25-29] In order to be called suitane the structure must have long limbs to be able to pass completely through the suit and thus ensure sufficient stability. Due to challenging synthetic approaches required to create suitanes they are rather rare examples of MIMs.

Very recently, Stoddart and co-workers have synthesized and characterized a novel member of suitanes family – suit[3]ane.[30] It contains a benzotrithiophene (**BTT**) derivative with three *n*-hexane substituents (**BTT-3C$_6$**) as a body and 3-fold symmetric pyridinium-based cage, namely HexaCage^{6+} (**HC^{6+}**), as a suit. Thus, [3] indicates the number of limbs protruding from the suit. **HC^{6+}** has a diameter of about 11 Å and provides a sufficiently large binding surface to interact with aromatic torso in the cavity *via* π···π interactions. The single crystal data have confirmed that **HC^{6+}·6PF$_6^-$⊃BTT-3C$_6$** (suit[3]ane) complex has a sandwich-like structure, in which **BTT-3C$_6$** is located between two hexameric platforms of **HC^{6+}** with plane-to-plane orientation (Figure 1). Note that **BTT-3C$_6$** unit is not perfectly centered with respect to the hexameric platform. NMR experiments revealed a strong binding between host and guest (K_a = 9.20·10^4 M^{-1}L).[30] Suit[3]ane shows high stability in acetonitrile at 100 °C for a period of 7 days.

Here we report a comprehensive analysis of photoinduced electron transfer (PET) processes occurring in **HC^{6+}·6PF$_6^-$⊃BTT-3C$_6$** (suit[3]ane) and a number of similar complexes using DFT/TDDFT theory. A conductor-like polarizable continuum model (CPCM) was applied to account for environmental effects. Non-covalent interactions between the subunits were explored using the energy decomposition analysis. Topological analysis was carried out with the Bader atom in molecules theory (QTAIM). Our results demonstrate that **HC^{6+}·6PF$_6^-$** cage can act as a strong electron acceptor, and suit[3]anes built from this cage and polycyclic aromatic guests exhibit pronounced PET properties.

Computational Methods

Geometry optimizations were performed employing the DFT BLYP[31,32] exchange–correlation functional with Ahlrichs' def2-SVP basis set,[33,34] and using the resolution of identity approximation (RI, alternatively termed density fitting)[35,36] implemented in the ORCA 4.1.2 program.[37,38] Canonical energy decomposition analysis (EDA) was calculated using the Amsterdam Density Functional (ADF) program.[39] Electronic structures calculations and vertical excitation energies were calculated using TDA formalism[40] with the range-separated functional from Handy and coworkers' CAM-B3LYP[41] and Ahlrichs' def2-SVP basis set,[33,34] using Gaussian 16 (rev. A03).[42] The empirical dispersion D3 correction with Becke–Johnson damping,[43,44] was employed. The population analysis performed within Mulliken,[45,46] Löwdin,[47] Hirshfeld,[48] CM5,[49] schemes were carried out using code implemented in Gaussian 16. The topological analysis of the electron density distribution was conducted using the "Quantum Theory of Atoms in Molecules" (QTAIM).[50,51] Electron density properties measured at the bond critical point (saddle point on electron density curvature corresponding to a minimum in the direction of the atomic interaction line and a maximum in two perpendicular directions) give information about the character of different chemical bonds.[52-54] The AIMALL suite of programs[55] was applied to evaluate the bond critical point properties and associated bond descriptors – the electron density [$\rho(r)$] in BCP, its Laplacian [$\nabla^2\rho(r)$], potential energy density [$V(r)$], kinetic energy density [$G(r)$], and total electron energy density [$H(r)$]. To visualize molecular structures and frontier molecular orbitals, Chemcraft 1.8. program[56] was used. Details of the methods used in this work, including analysis of excited states and solvent effects, calculation of electron transfer rates, reorganization and interaction energies are provided in Supporting Information.

Results and Discussion

Ground state properties

BTT has a planar sulfur-rich π-system formed by fused terthiophene. It has proven to be a useful donor in high performing organic photovoltaics.[57] In turn, **HC^{6+}** is an extended π-electron deficient pyridinium-based cyclophane platform with a large cavity capable to accommodate polycyclic aromatic guests. The combination of the strong donor and acceptor in one unit prompts us to study the response of the complex to photoexcitation. We have considered 1:1 complexes of **$HC^{6+}\cdot 6PF_6^-$** cage with **BTT** and its trihexyl derivative **BTT-3C$_6$**. The ground state (GS) geometries of the complexes (Figure 1) were optimized using BLYP-D3(BJ)/def2-SVP level of theory (see computational details in the SI).

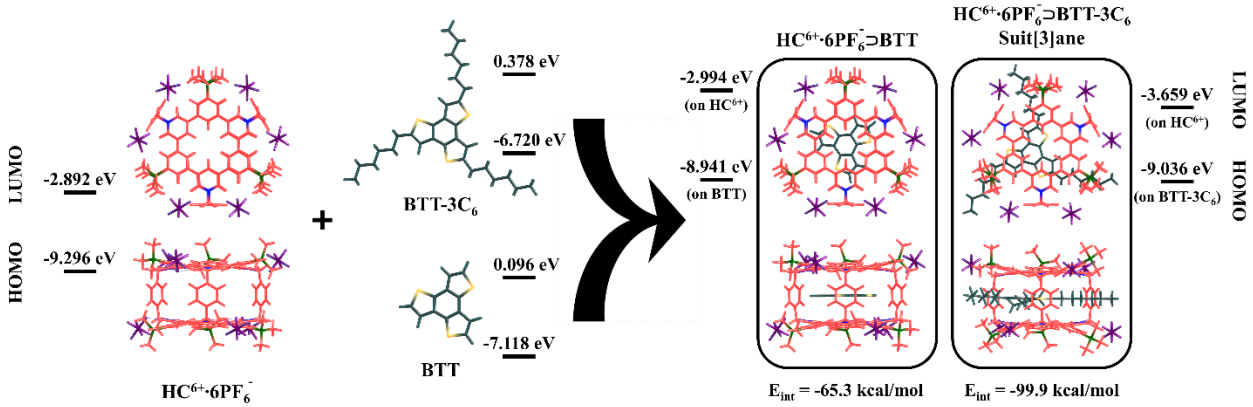

Figure 1. Structure of **$HC^{6+}\cdot 6PF_6^-\supset$BTT** and **$HC^{6+}\cdot 6PF_6^-\supset$BTT-3C$_6$**. HOMO and LUMO energies of the separated donor and acceptor, and their complexes.

As seen in Figure 1, HOMO and LUMO in both complexes are localized on **BTT** and **HC^{6+}** units, correspondingly. The energy of HOMO of benzotrithiophenes decreases dramatically (almost by 2 eV) by the formation of the complex. Taking into account the fact that **$HC^{6+}\cdot 6PF_6^-\supset$BTT** and **$HC^{6+}\cdot 6PF_6^-\supset$BTT-3C$_6$** are donor-acceptor complexes, we first checked the charge separation between the host and guest units in the GS. The population analysis performed within most popular schemes (Table S1, SI) did not reveal any notable charge transfer between the fragments. This means that the changes in HOMO energies are mainly caused by the electrostatic effect of the **$HC^{6+}\cdot 6PF_6^-$** cage, which contains positively and negatively charged regions (pyridinium subunits and hexafluorophosphates, respectively). Because the pyridinium centers are closer to **BTT**, a decrease of the HOMO energy of BTT is expected. To check this assumption, we calculated the orbital energies of **BTTs** in the field of point charges. To this aim the atoms of the cage were replaced by their Mulliken charges. Additionally, we compared the orbital energies of **BTT** and **BTT-3C$_6$** computed using their geometries both in the isolated state and in the complexes. The calculations showed that the electrostatic effects are responsible for the shift of the orbital energies of BTTs, while the effect of the geometry relaxation is almost negligible. We note that the formation of **$HC^{6+}\cdot 6PF_6^-\supset$BTT-3C$_6$** is also accompanied by significant changes in LUMO energy of **$HC^{6+}\cdot 6PF_6^-$** cage. It decreases from -2.89 eV in the free cage to -3.66 eV in the complex. However, the LUMO energies of **$HC^{6+}\cdot 6PF_6^-$** remain almost unchanged by the formation of the **$HC^{6+}\cdot 6PF_6^-\supset$BTT** complex (Table S2). This difference may be explained by geometrical features of **$HC^{6+}\cdot 6PF_6^-\supset$BTT-3C$_6$**. In contrast to **$HC^{6+}\cdot 6PF_6^-\supset$BTT**, in which the symmetry axes of **BTT** and the cage coincide, the axes of **BTT-3C$_6$** and **$HC^{6+}\cdot 6PF_6^-$** do not match because **BTT-3C$_6$** unit is shifted from the center of the cage.

To estimate the stability of the complexes, the interaction energy (ΔE_{int}) between **$HC^{6+}\cdot 6PF_6^-$** cage and benzotrithiophene units was computed. For **$HC^{6+}\cdot 6PF_6^-\supset BTT$** and **$HC^{6+}\cdot 6PF_6^-\supset BTT\text{-}3C_6$** complexes, ΔE_{int} was found to be -65.26 and -99.93 kcal/mol, correspondingly. To analyze the nature of the host-guest interactions, we performed the Morokuma-like energy decomposition analysis (EDA)[58] implemented in the ADF program.[59] The EDA decomposes the interaction energy into four components: electrostatic (ΔE_{elstat}), Pauli repulsion (ΔE_{Pauli}), orbital interactions (ΔE_{oi}), and dispersion corrections (ΔE_{disp}), and allows one to estimate the role of the specific interactions. The EDA results listed in Table S3 indicate that the host-guest interactions in the complexes are quite similar. The destabilizing term (ΔE_{Pauli}) is equal to 65.0 and 122.1 kcal/mol for **BTT-** and **$BTT\text{-}3C_6$**–based complexes, respectively. Among the binding forces ($\Delta E_{elstat} + \Delta E_{oi} + \Delta E_{disp}$), the dispersion term prevails with the contribution of 64 and 60% for **$HC^{6+}\cdot 6PF_6^-\supset BTT$** and **$HC^{6+}\cdot 6PF_6^-\supset BTT\text{-}3C_6$**. The second largest term is electrostatic attraction with equal contribution of 25% for both complexes. Finally, the orbital interactions provide only 11 and 15% of the total stabilization interactions. The larger ΔE_{oi} in **$HC^{6+}\cdot 6PF_6^-\supset BTT\text{-}3C_6$** correlates with smaller HOMO-LUMO gap as compared with **$HC^{6+}\cdot 6PF_6^-\supset BTT$** (Figure 1).

To gain access to the host-guest interaction topology, we performed a series of QTAIM calculations.[50] The electron density, its Laplacian, bond critical points (BCPs) and other topological parameters were considered (see Table S4). The analysis revealed two types of host-guest interactions: $\pi\cdots\pi$ interactions between π-electron systems of the subunits, and CH$\cdots\pi$ interactions between the fragments. In the case of **$HC^{6+}\cdot 6PF_6^-\supset BTT$**, $\pi\cdots\pi$ interactions are dominant. Replacing of **BTT** with **$BTT\text{-}3C_6$** unit and its shift from the center of the cage affect significantly the interaction topology. Such a mutual arrangement of the cage and hexyl substituents of benzotrithiophene in **$HC^{6+}\cdot 6PF_6^-\supset BTT\text{-}3C_6$** provides a larger number of BCPs of both types, maintaining comparable electron density characteristics. The number of BCPs corresponding to $\pi\cdots\pi$ interactions is slightly larger compared to **$HC^{6+}\cdot 6PF_6^-\supset BTT$** (14 vs 12), while the number of BCPs indicating CH$\cdots\pi$ interactions is significantly larger (24 vs 9). Note that characteristics of BCPs in **$HC^{6+}\cdot 6PF_6^-\supset BTT$** and **$HC^{6+}\cdot 6PF_6^-\supset BTT\text{-}3C_6$** complexes are similar (Table S4). Because the main difference in the number of BCPs is due to critical points corresponding to the CH$\cdots\pi$ interactions, we can assume that this type of interactions is responsible for increasing the interaction energy between the fragments in **$HC^{6+}\cdot 6PF_6^-\supset BTT\text{-}3C_6$** compared to **$HC^{6+}\cdot 6PF_6^-\supset BTT$**. QTAIM molecular graphs for **$HC^{6+}\cdot 6PF_6^-\supset BTT$** and **$HC^{6+}\cdot 6PF_6^-\supset BTT\text{-}3C_6$** complexes are given in Figure S1, SI.

Analyzing the results of crystallographic measurements for **$HC^{6+}\cdot 6PF_6^-\supset BTT$** and **$HC^{6+}\cdot 6PF_6^-\supset BTT\text{-}3C_6$**, an interesting feature of **$HC^{6+}\cdot 6PF_6^-\supset BTT$** complex was identified. In particular, we noticed that its X-ray structure indicates the presence of a pronounced **BTT** unit disarray, which is apparently a superposition of **BTT** reflection and dynamic positional disorder (Figure 2a-c). This type of disorder usually appears because of thermally induced motions. Since the X-ray experiment was carried out at 100 K, this disorder is most likely the result of a low-energy barrier to the rotation of the **BTT** unit inside the cage. To assess the thermally accessible amplitude of rotation, a corresponding rotational scan was performed. For **$HC^{6+}\cdot 6PF_6^-\supset BTT$**, the centers of mass of the host and guest coincide. Thus, we computed the energy of the complex as a function of the angle ϕ between vectors A and B (Figure 2d). Vector A goes from the center of mass to the middle of the *p*-xylene linker which connects two hexameric platforms. Vector B starts at the same center of mass and passes through the α-proton of the thiophene ring. Since the complex has a symmetry close to C_3, the scan of the angle ϕ was performed from -4° to 127° with a step of 3°.

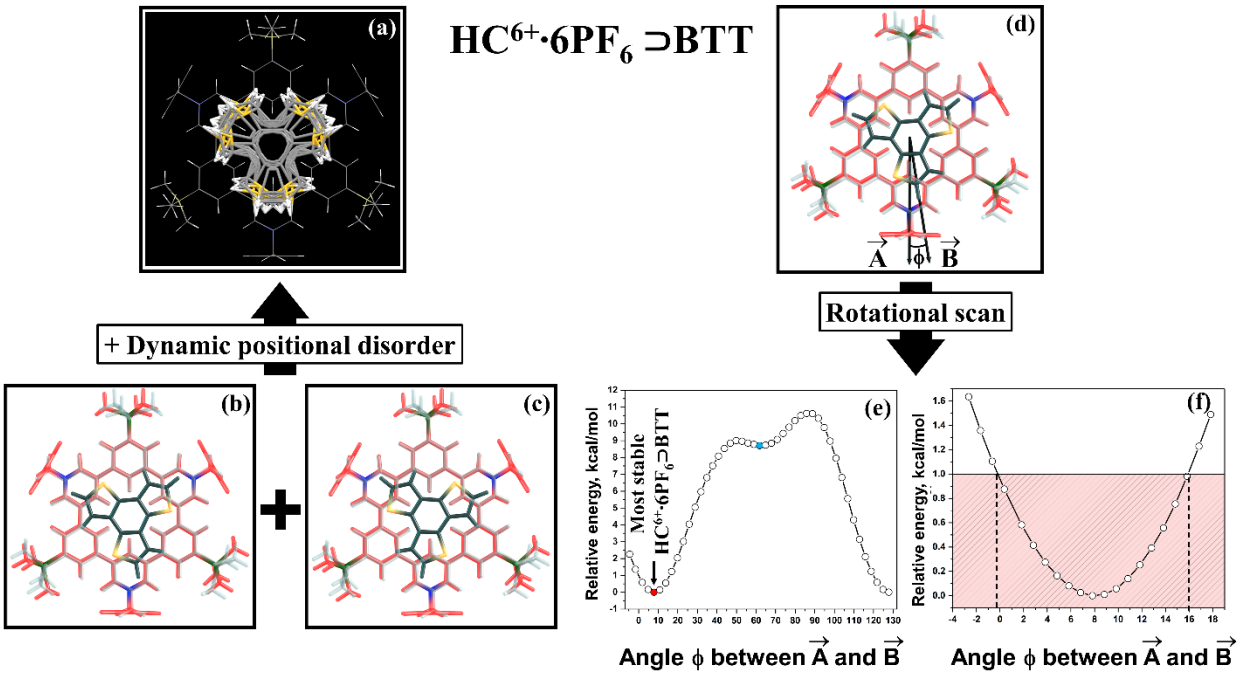

Figure 2. (a) Crystal structure of **HC^{6+}·6PF_6^-⊃BTT** complex (**PF_6^-** units have been omitted for clarity). Data taken from CCDC data base (deposition number 2045036); (b) and (c) Two stereoisomers of **HC^{6+}·6PF_6^-⊃BTT** with clockwise and counterclockwise orientation of BTT fragment; (d) Vectors A and B used to define the rotational angle; (e) Dependence of the potential energy on the angle ϕ ranging from -4° to 127° with a step of 3°. The red and blue dots indicate two conformers; (f) Potential energy scan for the angle ϕ varying from -4° to 18° with a step of 1°. The relative energy remains within 1 kcal/mol when the angle ϕ varies between 0° and 16° (the region is highlighted in red).

We found that the rotation of **BTT** inside **HC^{6+}·6PF_6^-** cage occurs through a moderate energy barrier. We have identified two conformers. The first corresponds to the structure found in the solid state, with the α-proton of the thiophene ring pointing towards the phenyl linker (red dot in Figure 2e). In the second conformer (blue dot in Figure 2e), the α-proton is located between p-xylene linkers connecting two hexameric platforms. The energies of the conformers differ by 8.5 kcal/mol, the former being more stable. Their structures are shown in Figure S2. Scanning (Figure 2e) shows that the energy barrier for **BTT** rotation within 16° is less than 1 kcal/mol. This explains the disorder of **BTT** fragment observed in the crystallographic experiment for **HC^{6+}·6PF_6^-⊃BTT** complex.

Singlet excited states and role of PF_6^- counterions

Our results show that **HC^{6+}·6PF_6^-** cage in both complexes is characterized by a rather low LUMO energy, -2.99 and -3.66 eV (Figure 1) and can act as a good electron acceptor, while benzotrithiophenes are used as electron donors in organic optoelectronics.[60] Thus, suit[3]anes are expected to be prone to PET. Simulations of the excited states were carried out by TD-DFT method at the CAM-B3LYP-D3(BJ)/def2-SVP//BLYP-D3(BJ)/def2-SVP level of theory (see SI for computational details). To characterize the properties of excited states, **HC^{6+}·6PF_6^-⊃BTT** and **HC^{6+}·6PF_6^-⊃BTT-3C_6** systems were divided into 2 fragments: host (acceptor) **HC^{6+}·6PF_6^-** cage and guest (donor) **BTT** or **BTT-3C_6**. The electron density distribution was analyzed for the 100 lowest-lying excited states. Three types of excited states were

identified: (1) locally excited (LE) states, where excitation is mostly localized either on the guest (LE^{Guest}) or the host molecule (LE^{Host}) and charge separation is smaller than 0.1 ***e*** (CS < 0.1 ***e***); (2) charge transfer (CT) states showing significant charge separation (CS > 0.8 **e**); and (3) mixed states where both LE and CT states contribute substantially (0.1 ***e*** < CS < 0.8 ***e***).

In the gas phase, the 100 lowest-lying vertical singlet excitation energies of **HC^{6+}·6PF_6^-⊃BTT** complex vary from 4.02 to 5.43 eV (Table 1). The first excited state at 4.02 eV is the LE^{Host} state formed by the HOMO-2 → LUMO transition. LE^{Guest} states with exciton localization on **BTT** were not found within the 100 computed excited states. The lowest CT state with 0.89 ***e*** transferred from **BTT** to **HC^{6+}·6PF_6^-** lies only 0.1 eV higher in energy, at 4.12 eV, and corresponds to the HOMO → LUMO transition. It can be described as **[HC^{6+}·6PF_6^-]$^-$⊃[BTT]$^+$**. Among the studied excited states, only this type of charge separated state was observed.

The energies of the 100 lowest-lying singlet excited states of **HC^{6+}·6PF_6^-⊃BTT-3C_6** are shifted by 0.4 eV in comparison with **HC^{6+}·6PF_6^-⊃BTT** and vary from 3.62 to 5.02 eV. The energy of LE^{Host} states in both complexes is almost identical. But unlike **HC^{6+}·6PF_6^-⊃BTT**, the lowest excited state in **HC^{6+}·6PF_6^-⊃BTT-3C_6** is the CT state rather than LE^{Host}. This CT state is formed due to electron transfer from **BTT-3C_6** to **HC^{6+}·6PF_6^-** and can be described as the HOMO → LUMO transition. The frontier MOs representing the LE and CS states are shown in Figures S3-S4.

Table 1. Excitation energies (E_x, eV), main singly excited configuration (HOMO(H)–LUMO(L)) and its weight (W), oscillator strength (f), extent of charge transfer (CT, e) or localization of exciton (X) computed for neutral **HC^{6+}·6PF_6^-⊃BTT** and **HC^{6+}·6PF_6^-⊃BTT-3C_6** complexes, as well as for the charged **HC^{6+}⊃BTT** and **HC^{6+}⊃BTT-3C_6** complexes (data given in *italic*) in the gas-phase (VAC) and acetonitrile (ACN).

	Supramolecular host-guest systems					
	without PF_6^- counterions		**with PF_6^- counterions**			
	HC^{6+}⊃BTT	**HC^{6+}⊃BTT-3C_6**	**HC^{6+}·6PF_6^-⊃BTT**		**HC^{6+}·6PF_6^-⊃BTT-3C_6**	
	VAC		VAC	ACN	VAC	ACN
	LE^{Host} (**HC^{6+}/HC^{6+}·6PF_6^-**)					
E_x	*4.036*	*4.010*	4.018	4.143	4.072	4.187
Transition (W)	*H-8 – L (0.27)*	*H-11 – L (0.23)*	H-2 – L (0.32)	H-3 – L+3 (0.32)	H-7 – L (0.22)	H-3 – L (0.17)
f	*<0.001*	*<0.001*	0.002	0.027	0.004	0.003
X	*0.976*	*0.893*	0.969	0.965	0.899	0.928
	Most absorptive transition					
E_x	*4.778**	*4.781**	4.747*	4.817	4.964*	5.119*
Transition (W)	*H-1 – L+6 (0.17)*	*H-1 – L+13 (0.09)*	H – L+8 (0.08)	H-10 – L+8 (0.09)	H-6 – L+5 (0.05)	H-13 – L+2 (0.07)
f	*0.733*	*0.612*	0.238	1.315	0.362	1.164
Localization	***HC^{6+}***	***HC^{6+}***	**HC^{6+}·6PF_6^-**	**HC^{6+}·6PF_6^-**	**HC^{6+}·6PF_6^-**	**HC^{6+}·6PF_6^-**
X	*0.546*	*0.758*	0.807	0.882	0.739	0.720
CT	*0.389*	*0.128*	0.162	0.056	0.243	0.188
	CT (**BTT/BTT-3C_6 → HC^{6+}/HC^{6+}·6PF_6^-**)					
E_x	*4.236*	*3.546*	4.121	3.764	3.619	3.557

Transition (W)	*H-1 – L+1 (0.39)*	*H – L (0.57)*	H – L (0.81)	H – L (0.85)	H – L (0.74)	H – L (0.72)
f	*0.002*	*0.010*	< 0.001	< 0.001	0.014	0.0015
CT	*0.800*	*0.914*	0.890	0.952	0.917	0.937

* - mixed states with significant contributions of both LE and CT.

The energetics of CT states can be strongly affected by charged species. This was demonstrated experimentally and theoretically by the example of the inclusion complex [10]CPP⊃Li^+@C_{60},[61,62] Li^+-doped carbon nano-onions,[63] and the Zn-porphyrin–[10]CPP⊃C_{60} junction.[64] A reliable prediction of the structure for solvated contact ion pairs is still very challenging task. Thus, we studied the role of **PF_6^-** counterions on the excitations and electron transfer properties of the isolated **HC^{6+}·6PF_6^-⊃BTT** and **HC^{6+}·6PF_6^-⊃BTT-3C_6** complexes. The geometries of both complexes without the **PF_6^-** counterions were optimized. Our calculation of the complexes with and without **PF_6^-** revealed only minor differences in predicted electronic properties. In particular, the energy of LE states remains almost unchanged (it varies within 0.1 eV). The absence of the influence of counterions on the energetics of LE states seems reasonable. Vertical GS → LE transition are not associated with a significant redistribution of the electron density and, its electrostatic interaction in the GS and LE states with counterions is similar. In contrast, charge separation between the fragments in CT states can lead to significant electrostatic effects. However, in our systems, these effects are rather small (slightly exceeding 0.1 eV) due to the symmetric arrangement of the PF_6^- counterions. Because of that, some inaccuracies in the positions of the counterions will not significantly affect the energetics of excited states in the complexes.

Effects of environment

To get insight into the influence of polar environment on electronic excitations, a well-proven COSMO-like model[64-67] with acetonitrile as a solvent was applied. The dipole moment of **HC^{6+}·6PF_6^-⊃BTT** and **HC^{6+}·6PF_6^-⊃BTT-3C_6** was calculated to be 0.20 and 1.13 D, respectively. The very small dipole moment of **HC^{6+}·6PF_6^-⊃BTT** can be explained by the C_3 symmetry of this system. The dipole moment of **HC^{6+}·6PF_6^-⊃BTT-3C_6** is slightly bigger due to the fact that the encapsulated **BTT-3C_6** unit is shifted from the center of the cage. Since the complexes have positively and negatively charged regions (pyridinium subunits and hexafluorophosphates), they have high solvation energies, -3.40 and -6.33 eV were computed for **HC^{6+}·6PF_6^-⊃BTT** and **HC^{6+}·6PF_6^-⊃BTT-3C_6**, correspondingly. This difference in solvation prompted us to carefully compare the structural elements of the complexes. It can be expected that the mutual arrangement of pyridinium groups and hexafluorophosphate anions is responsible for the change in the solvation energy. Indeed, the geometry analysis revealed that the average distance between phosphorus atom of **PF_6^-** anion and closest pyridinium nitrogen atom in **HC^{6+}·6PF_6^-⊃BTT** is 4.417 Å, while in **HC^{6+}·6PF_6^-⊃BTT-3C_6** this value is 4.883 Å. The observed difference seems to be due to the fact that three n-hexyl chains of **BTT-3C_6** fragment extending beyond the cage cause repulsion of the **PF_6^-** anions. In turn, the greater distance between the oppositely charged centers in **HC^{6+}·6PF_6^-⊃BTT-3C_6** leads to better solvation of each fragment, and thus facilitates the solvation of the complex. To confirm this assumption we removed the **PF_6^-** counterions and recalculated the solvation energies for **HC^{6+}⊃BTT** and **HC^{6+}⊃BTT-3C_6**. Their absolute difference became significantly smaller, instead of 2.93 eV we obtained 0.78 eV.

The change in the dipole moments when going from the GS to the LE^{Host} states is found to be rather small; even for **HC^{6+}·6PF_6^-⊃BTT-3C_6** it does not exceed 2.5 D. The calculated solvation energies of the GS and LE^{Guest} states are also very similar. Detailed data for both complexes are given in Table S5, SI. The dipole

moment of CT states is usually significantly larger than that of GS and LE states. However, the high ability of both fragments to delocalize the excess charge and the high symmetry of the complexes are the reason for a relatively small difference (less than 4.2 D) in the dipole moments found for the GS and CT states. Solvation of the complexes leads to stabilization of CT states and their relative energy reduces from 4.12 to 3.76 eV, and from 3.62 to 3.56 eV for **$HC^{6+}\cdot 6PF_6^-\supset BTT$** and **$HC^{6+}\cdot 6PF_6^-\supset BTT\text{-}3C_6$**, respectively. Important to note that stabilization of CT state in **$HC^{6+}\cdot 6PF_6^-\supset BTT$** is sufficient to reorder LE and CT states (Figure 3a). Thus, in polar solvent the charge transfer state is the lowest-lying excited state for both complexes. A comparison of the measured and predicted UV-Vis spectra demonstrates a good agreement between theory and experiment (Figure 3b). This, in turn, indicates that the chosen computational method is well suited for the systems under consideration.

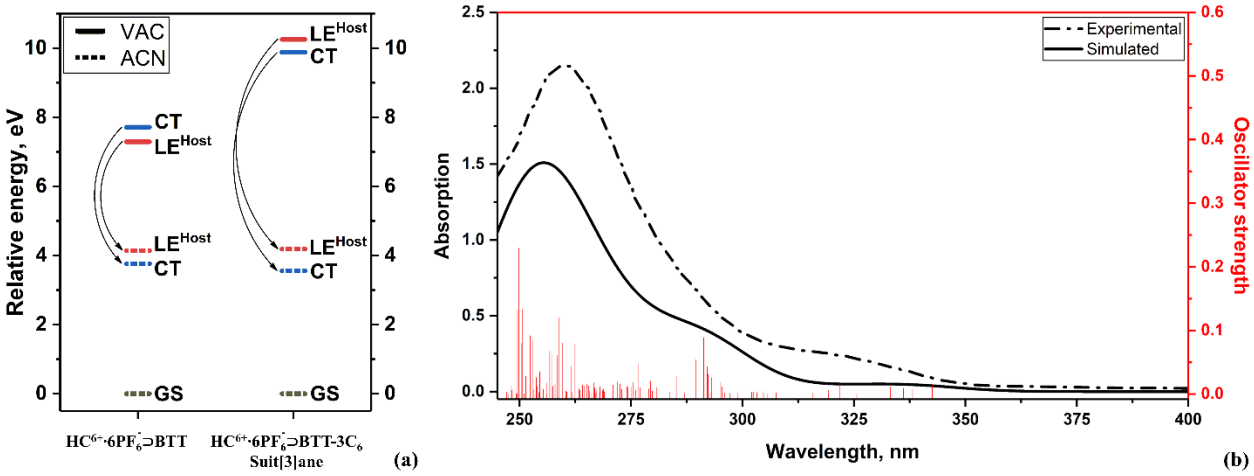

Figure 3. (a) Energies of LE and CT states (in eV) computed for **$HC^{6+}\cdot 6PF_6^-\supset BTT$** and **$HC^{6+}\cdot 6PF_6^-\supset BTT\text{-}3C_6$** in vacuum (VAC) and acetonitrile (ACN); (b) Experimental (dash line) and simulated (solid line) spectra of **$HC^{6+}\cdot 6PF_6^-\supset BTT\text{-}3C_6$** (suit[3]ane) in ACN. The simulated absorption spectrum was constructed using Gaussian broadening (FWHM=0.17 eV). Red vertical lines show the oscillator strength for the 100 lowest-lying singlet excited states. The experimental UV-Vis spectrum is taken from ref. 30.

Singlet excited states of aggregates

The strong stabilization of the CT state and the presence of strongly light-absorbing states suggest a possible application of **$HC^{6+}\cdot 6PF_6^-\supset BTT$** and **$HC^{6+}\cdot 6PF_6^-\supset BTT\text{-}3C_6$** host-guest complexes in photovoltaics. Note that the properties considered above were obtained for individual molecules and thus the intermolecular interaction was not taken into account. In order to gain an insight into the effect of attraction aggregation on the electron transfer processes, we applied the cluster approach to modeling the properties of aggregated states. Let us consider now several systems consisting of one (**U1**), two (**U2**) or three (**U3**) units **$HC^{6+}\cdot 6PF_6^-\supset BTT$** (Figure 4). Both linear (**U3L**) and triangle (**U3T**) geometries were studied for clusters consisting of three units. The mutual arrangement of the units were taken from the X-ray data.[30]

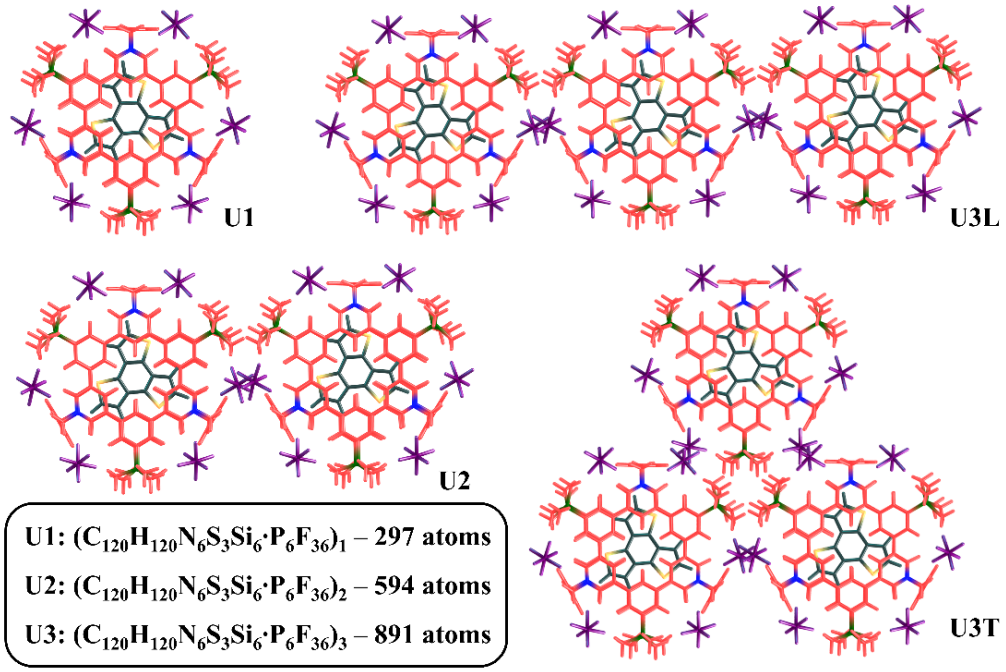

Figure 4. Structure of the considered **$HC^{6+} \cdot 6PF_6^- \supset BTT$** clusters .

Excited state properties of these clusters were calculated using the sTDA method introduced by Grimme.[68] The TDDFT approach is known to be feasible for medium-sized systems.[69] However, its applicability to systems with more than 5000 atomic basis functions is extremely time-consuming. Another problem with large systems is the high density of the electronic states, which may cause the instability of the Davidson algorithm usually applied for excited state calculations. The use of sTDA makes it possible to overcome these difficulties. The great performance of sTDA has been demonstrated for various organic systems[68,70] and carbon-rich materials.[63] To test the applicability of sTDA to the suit[3]anes, we compare the results obtained with both sTDA and conventional TDDFT/CAM-B3LYP (Table 2).

Table 2. Excitation energies (E_x, eV), main singly excited configuration (HOMO(H)–LUMO(L)) and its weight (W), the extent of charge transfer (CT, e) and exciton localization (X), the HOMO and LUMO energies and HOMO-LUMO (HL) gap computed in the neutral clusters **U1**-**U3**.

	Clusters of **$HC^{6+} \cdot 6PF_6^- \supset BTT$**				
	TDDFT	**sTDA**			
	U1	**U1**	**U2**	**U3L**	**U3T**
H	-8.94	-8.93	-8.90	-8.88	-8.87
L	-2.99	-2.98	-3.01	-3.01	-2.93
HL	5.95	5.95	5.89	5.87	5.94
	LE^{Host} **($HC^{6+} \cdot 6PF_6^-$)**				
E_x	4.018	4.019	4.018	4.052	4.066
Transition (W)	H-2 – L (0.32)	H-2 – L (0.35)	H-6 – L+1 (0.30)	H-6 – L+5 (0.45)	H-6 – L+4 (0.15)
X	0.969	0.960	0.951	0.964	0.940

	CT (**BTT** → **HC^{6+}·6PF$_6^-$**)				
E_x	4.121	4.177	4.120	4.155	4.198
Transition (W)	H – L (0.81)	H – L (0.85)	H – L+1 (0.72)	H-1 – L+1 (0.82)	H-2 – L (0.60)
CT	0.890	0.892	0.918	0.922	0.855

As seen in Table 2, the TDDFT and sTDA results for **U1** are very close. Because of that, we applied the simplified DFT method to the other complexes. The computations predict very similar electronic properties for all aggregates. The changes in the HOMO and LUMO energies do not exceed 0.1 eV. The similar electronic structure of the clusters is reflected in almost identical energies for LE and CT states. In all cases, the lowest LE state is localized on **HC^{6+}·6PF$_6^-$** host cage. Within the 140 lowest excited states, only CT states are observed that correspond to the electron transfer from BTT to **HC^{6+}·6PF$_6^-$** within a single unit, i.e. no charge separation is found between the units. The similarity of excited state of the clusters suggest that the behavior of **HC^{6+}·6PF$_6^-$⊃BTT** by low energy excitation in aggregation state hardly differs from that which we observe in a single unit.

Encapsulation of other molecules by HC^{6+}·6PF$_6^-$ cage and electron transfer rates

The electron-withdrawing properties of **HC^{6+}·6PF$_6^-$**, as well as its ability to delocalize charge makes this cage a promising candidate for photovoltaic applications. The large cavity between two hexameric platforms allows for the accommodation of various polycyclic aromatic guests. Such aromatic systems have developed into an important class of materials with broad application potential in organic electronic components.[71-73] Of particular interest are C3-symmetric planar systems that are stable, exceptionally soluble and easy to modify.[74-77] We studied PET processes occurring in several inclusion complexes formed by **HC^{6+}·6PF$_6^-$** moiety and an aromatic partner with a 3-fold symmetry. The electron-donating ability of the guest (assessed by its HOMO energy in the complex) decreases in the order: thiatruxene (**TruxS**); benzotrithiophenes (**BTT** and **BTT-3C$_6$**); benzotrifuran (**BTF**); benzotristhiazole (**BTTZ**) and benzotrisoxazole (**BTOZ**). The guest molecules and the structure of the host-guest complexes are shown in Figure 5.

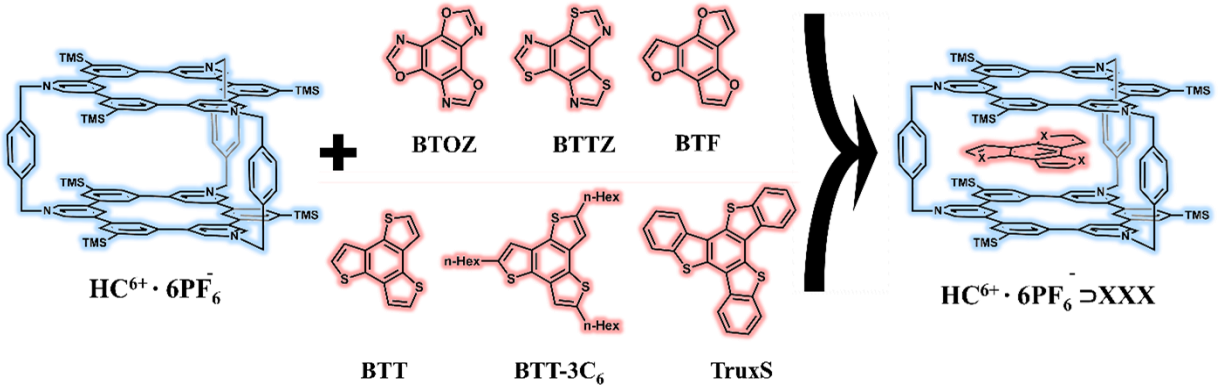

Figure 5. Structures of **HC^{6+}·6PF$_6^-$** host, selected guest molecules, and inclusion complexes **HC^{6+}·6PF$_6^-$⊃XXX**. **PF$_6^-$** anions have been omitted for clarity.

Geometry optimization of the complexes and calculation of their excited state properties were performed as described earlier. The data for the LE and CT states are given in Table S6, the solvation energies are listed in Table S7. The GS → CT transitions have typically a very weak oscillator strength, and thus the CT states cannot be well populated directly by light absorption. However, they can be generated by a decay of LE states. The rates of electron transfer k_{ET} were calculated using the semi-classical method by Ulstrup and Jortner.[78,79] Within this approach, the intramolecular relaxation associated with ET is described by an effective vibrational mode, and the rate is controlled by four parameters: electronic coupling V_{ij} of the initial and final states, solvation reorganization energy λ_s, reaction Gibbs energy ΔG^0, and effective Huang-Rhys factor, S_{eff}. The computed parameters, as well as k_{ET} rates in ACN solvent for all studied systems are listed in Table 3. The rates were obtained using the effective frequency of 1600 cm^{-1}, which corresponds to the stretching of C=C bonds. As seen from Table S8, the computed ET rates do not change significantly when the effective frequency varies in a fairly wide range.

Table 3. Ground and excited state properties, and electron transfer parameters computed for the complexes **$HC^{6+}\cdot 6PF_6^-$⊃XXX**: interaction energy (ΔE_{int}, kcal/mol), HOMO energy of encapsulated fragment **XXX** (HOMO, eV), excitation energy of the lowest LE (E_X, eV), exciton localization (X) on **$HC^{6+}\cdot 6PF_6$** fragment, extent of charge transfer (CT, e), Gibbs energy (ΔG^0, eV), electronic coupling ($|V_{ij}|$, eV), internal and solvent reorganization energies (λ_I and λ_s, eV), and electron transfer rate (k_{ET}, s^{-1}).

	$HC^{6+}\cdot 6PF_6^-$ ⊃XXX	ΔE_{int}	HOMO of **XXX**	E_X[a]	CT[b]	ΔG^0 [c]	$\lvert V_{ij}\rvert$	Reorg. Energy		k_{ET}
								λ_i	λ_s	
1	**TruxS**	-99.5	-8.42	E=4.07 X=0.89	E=3.88 CT=0.93	-0.19	$2.47\cdot 10^{-3}$	0.161	0.111	$2.05\cdot 10^{11}$
2	**BTT**	-65.3	-8.94	E=4.14 X=0.97	E=3.76 CT=0.95	-0.38	$1.16\cdot 10^{-3}$	0.171	0.166	$2.50\cdot 10^{10}$
3	**BTT-3C$_6$**	-99.9	-9.04	E=4.19 X=0.97	E=3.56 CT=0.95	-0.63	$1.95\cdot 10^{-3}$	0.175	0.124	$1.61\cdot 10^{10}$
4	**BTF**	-50.9	-9.12	E=4.23 X=0.99	E=4.04 CT=0.91	-0.19	$4.17\cdot 10^{-4}$	0.193	0.207	$6.57\cdot 10^{9}$
5	**BTTZ**	-55.2	-9.56	E=4.24 X=0.98	E=4.85 CT=0.80	+0.61	$8.05\cdot 10^{-4}$	0.196	0.117	[$2.6\cdot 10^{-9}$]
6	**BTOZ**	-42.0	-10.02	E=4.21 X=0.99	n/f [d]					

[a] The lowest LE states localized on the **$HC^{6+}\cdot 6PF_6^-$** cage; [b] electron transfer from **XXX** to **$HC^{6+}\cdot 6PF_6^-$**; [c] Gibbs energy of electron transfer LE → CT ; [d] CT states have not been found within the calculated excited states.

Our analysis revealed that the lowest LE state is located on **$HC^{6+}\cdot 6PF_6^-$** fragment in all complexes. The CT state corresponds to the electron transfer from the encapsulated heterocycle **XXX** to **$HC^{6+}\cdot 6PF_6^-$** cage. The PET in the complexes with **TruxS**, **BTT**, **BTT-3C$_6$**, and **BTF** is characterized by a negative Gibbs free energy in the range from -0.18 to -0.63 eV. The thermodynamically favorable electron transfer even in the case of a rather poor donor **BTF** (ΔG^0 = -0.19 eV) confirms the significant electron-withdrawing ability of the **$HC^{6+}\cdot 6PF_6^-$** cage. In benzotristhiazole-based complex, however, ΔG^0 =+0.61 eV and the electron transfer is energetically forbidden. We note that in the benzotrisoxazole complex, the CT states were not found within the 50 lowest-lying excited states. This suggests that the Gibbs energy for CT process is higher than 1 eV. The positive value of ΔG^0 makes the ET process in this complex unlikely. Our computations

confirmed that the ET rate for **$HC^{6+}\cdot 6PF_6^-\supset$BTTZ** is extremely low (Table 3). On the contrary, charge separation is efficient in **$HC^{6+}\cdot 6PF_6^-\supset$TruxS**, **$HC^{6+}\cdot 6PF_6^-\supset$BTT**, **$HC^{6+}\cdot 6PF_6^-\supset$BTT-3C$_6$**, and **$HC^{6+}\cdot 6PF_6^-\supset$BTF** complexes and occurs on picosecond timescale (the characteristic time is 5, 40, 62, and 152 ps, respectively).

In addition, we studied the influence of geometry relaxation on the reaction rate of charge separation in **$HC^{6+}\cdot 6PF_6^-\supset$BTT** in acetonitrile. The computed ΔG^0 values and electron transfer rates for the Franck-Condon (FC) and relaxed structures are presented in Table S9. The calculations showed small changes in the energy of LE and CT states (LE^{Host} changes from 4.14 to 4.20 eV and CT changes from 3.76 to 3.67 eV when moving from FC to relaxed geometry). Thus, the ΔG^0 changes by only 0.15 eV.

Conclusions

In this work, we have studied ground- and excited-state properties for a series of the newly reported suit[3]anes constructed from a polycyclic aromatic guest incorporated into the pyridinium-based cage **$HC^{6+}\cdot 6PF_6^-$**. The low LUMO of **$HC^{6+}\cdot 6PF_6^-$** and its ability to delocalize charge make this cage an efficient electron acceptor. The TDDFT results obtained for **$HC^{6+}\cdot 6PF_6^-\supset$XXX** inclusion complexes show that the photoinduced electron transfer process is favorable not only for complexes with strong donors, such as thiatruxene or benzotrithiophenes, but also for poor donors, such as benzotrifuran. The photo-induced charge separation occurs on a picosecond time scale. In contrast, the electron transfer does not occur in the complexes with electron deficient benzotristhiazole and benzotrisoxazole. The high stability of suit[3]anes in combination with their photoinduced electron transfer properties makes this new class of interlocked molecules promising materials for photovoltaic applications.

Conflicts of interest

There are no conflicts to declare.

Author contributions

A. J. S. Investigation, Formal analysis, Writing – original draft, Writing – review & editing
O. A. S. Investigation, Formal analysis, Writing – original draft, Writing – review & editing
M. S. Supervision, Writing – review & editing, Funding acquisition
A. A. V. Supervision, Writing – review & editing

Acknowledgements

We are grateful for financial support from the Spanish MINECO (Network RED2018-102815-T, project CTQ2017-85341-P, and Juan de la Cierva contract IJC2019-039846-I to A.J.S. and FJCI-2017-32757 to O.A.S.) and the Catalan DIUE (2017SGR39).

References

1. B. Taghavi Shahraki, S. Maghsoudi, Y. Fatahi, N. Rabiee, S. Bahadorikhalili, R. Dinarvand, M. Bagherzadeh and F. Verpoort, *Coord. Chem. Rev.*, 2020, **423**, 213484.
2. A. Martinez-Cuezva, A. Saura-Sanmartin, M. Alajarin and J. Berna, *ACS Catal.*, 2020, **10**, 7719-7733.
3. A. W. Heard and S. M. Goldup, *ACS Cent. Sci.*, 2020, **6**, 117-128.
4. M. C. J. P. Sauvage and C. Dietrich-Buchecker , *Rotaxanes and Knots: A Journey Through the World of Molecular Topology*, Wiley-VCH, Weinheim, 1999.
5. J. F. Stoddart, *Chem. Soc. Rev.*, 2009, **38**, 1802-1820.
6. E. Wasserman, *J. Am. Chem. Soc.*, 1960, **82**, 4433-4434.
7. H. L. Frisch and E. Wasserman, *J. Am. Chem. Soc.*, 1961, **83**, 3789-3795.
8. R. S. Forgan, J.-P. Sauvage and J. F. Stoddart, *Chem. Rev.*, 2011, **111**, 5434-5464.
9. C. Wolf, *Dynamic Stereochemistry of Chiral Compounds: Principles and Applications*, The Royal Society of Chemistry, Cambridge, 2008, pp. 444-479.
10. O. Lukin, A. Godt and F. Vögtle, *Chem. Eur. J.*, 2004, **10**, 1878-1883.
11. C. O. Dietrich-Buchecker, J. P. Sauvage and J. M. Kern, *J. Am. Chem. Soc.*, 1984, **106**, 3043-3045.
12. P. R. Ashton, T. T. Goodnow, A. E. Kaifer, M. V. Reddington, A. M. Z. Slawin, N. Spencer, J. F. Stoddart, C. Vicent and D. J. Williams, *Angew. Chem. Int. Ed.*, 1989, **28**, 1396-1399.
13. M. Fujita, F. Ibukuro, H. Hagihara and K. Ogura, *Nature*, 1994, **367**, 720-723.
14. S. Mena-Hernando and E. M. Pérez, *Chem. Soc. Rev.*, 2019, **48**, 5016-5032.
15. P. L. Anelli, N. Spencer and J. F. Stoddart, *J. Am. Chem. Soc.*, 1991, **113**, 5131-5133.
16. A. Harada, J. Li and M. Kamachi, *Nature*, 1992, **356**, 325-327.
17. H.-Y. Zhou, Q.-S. Zong, Y. Han and C.-F. Chen, *Chem. Commun.*, 2020, **56**, 9916-9936.
18. C. O. Dietrich-Buchecker and J.-P. Sauvage, *Angew. Chem. Int. Ed.*, 1989, **28**, 189-192.
19. D. A. Leigh, F. Schaufelberger, L. Pirvu, J. H. Stenlid, D. P. August and J. Segard, *Nature*, 2020, **584**, 562-568.
20. T. Kraus, M. Buděšínský, J. Cvačka and J.-P. Sauvage, *Angew. Chem. Int. Ed.*, 2006, **45**, 258-261.
21. Y. Lu, H.-N. Zhang and G.-X. Jin, *Acc. Chem. Res.*, 2018, **51**, 2148-2158.
22. C. J. Bruns and J. F. Stoddart, *The Nature of the Mechanical Bond: From Molecules to Machines*, Wiley, Hoboken, 2017, pp. 1-54.
23. J. F. Nierengarten, C. O. Dietrich-Buchecker and J. P. Sauvage, *J. Am. Chem. Soc.*, 1994, **116**, 375-376.
24. J. C. Loren, M. Yoshizawa, R. F. Haldimann, A. Linden and J. S. Siegel, *Angew. Chem. Int. Ed.*, 2003, **42**, 5702-5705.
25. A. R. Williams, B. H. Northrop, T. Chang, J. F. Stoddart, A. J. P. White and D. J. Williams, *Angew. Chem. Int. Ed.*, 2006, **45**, 6665-6669.
26. Y.-C. Wang, Y.-P. Liang, J.-Y. Cai, Y.-J. He, Y.-H. Lee and Y.-T. Chan, *Chem. Commun.*, 2016, **52**, 12622-12625.
27. K. Zhu, G. Baggi, V. N. Vukotic and S. J. Loeb, *Chem. Sci.*, 2017, **8**, 3898-3904.
28. A. Pun, D. A. Hanifi, G. Kiel, E. O'Brien and Y. Liu, *Angew. Chem. Int. Ed.*, 2012, **51**, 13119-13122.
29. W. Liu, C. L. Stern and J. F. Stoddart, *J. Am. Chem. Soc.*, 2020, **142**, 10273-10278.
30. X.-Y. Chen, D. Shen, K. Cai, Y. Jiao, H. Wu, B. Song, L. Zhang, Y. Tan, Y. Wang, Y. Feng, C. L. Stern and J. F. Stoddart, *J. Am. Chem. Soc.*, 2020, **142**, 20152-20160.
31. A. D. Becke, *Phys. Rev. A*, 1988, **38**, 3098-3100.
32. C. Lee, W. Yang and R. G. Parr, *Phys. Rev. B*, 1988, **37**, 785-789.
33. F. Weigend and R. Ahlrichs, *Phys. Chem. Chem. Phys.*, 2005, **7**, 3297-3305.
34. F. Weigend, *Phys. Chem. Chem. Phys.*, 2006, **8**, 1057-1065.

35. K. Eichkorn, O. Treutler, H. Öhm, M. Häser and R. Ahlrichs, Chem. *Phys. Lett.*, 1995, **240**, 283-290.
36. K. Eichkorn, F. Weigend, O. Treutler and R. Ahlrichs, *Theor. Chem. Acc.*, 1997, **97**, 119-124.
37. F. Neese, *Wiley Interdiscip. Rev.: Comput. Mol. Sci.*, 2012, **2**, 73-78.
38. F. Neese, *Wiley Interdiscip. Rev.: Comput. Mol. Sci.*, 2017, **8**, e1327.
39. ADF 2018, SCM, Theoretical Chemistry, Vrije Universiteit, Amsterdam, The Netherlands, http://www.scm.com.
40. S. Hirata and M. Head-Gordon, *Chem. Phys. Lett.*, 1999, **314**, 291-299.
41. T. Yanai, D. P. Tew and N. C. Handy, *Chem. Phys. Lett.*, 2004, **393**, 51-57.
42. M. J. Frisch, G. W. Trucks, H. B. Schlegel, G. E. Scuseria, M. A. Robb, J. R. Cheeseman, G. Scalmani, V. Barone, G. A. Petersson, H. Nakatsuji, X. Li, M. Caricato, A. V. Marenich, J. Bloino, B. G. Janesko, R. Gomperts, B. Mennucci, H. P. Hratchian, J. V. Ortiz, A. F. Izmaylov, J. L. Sonnenberg, D. Williams-Young, F. Ding, F. Lipparini, F. Egidi, J. Goings, B. Peng, A. Petrone, T. Henderson, D. Ranasinghe, V. G. Zakrzewski, J. Gao, N. Rega, G. Zheng, W. Liang, M. Hada, M. Ehara, K. Toyota, R. Fukuda, J. Hasegawa, M. Ishida, T. Nakajima, Y. Honda, O. Kitao, H. Nakai, T. Vreven, K. Throssell, J. A. Montgomery, Jr., J. E. Peralta, F. Ogliaro, M. J. Bearpark, J. J. Heyd, E. N. Brothers, K. N. Kudin, V. N. Staroverov, T. A. Keith, R. Kobayashi, J. Normand, K. Raghavachari, A. P. Rendell, J. C. Burant, S. S. Iyengar, J. Tomasi, M. Cossi, J. M. Millam, M. Klene, C. Adamo, R. Cammi, J. W. Ochterski, R. L. Martin, K. Morokuma, O. Farkas, J. B. Foresman, and D. J. Fox, Gaussian 16, Revision A.03, Gaussian Inc., Wallingford CT, 2016.
43. S. Grimme, J. Antony, S. Ehrlich and H. Krieg, *J. Chem. Phys.*, 2010, **132**, 154104.
44. S. Grimme, S. Ehrlich and L. Goerigk, *J. Comput. Chem.*, 2011, **32**, 1456-1465.
45. R. S. Mulliken, *J. Chem. Phys.*, 1955, **23**, 1833-1840.
46. R. S. Mulliken, *J. Chem. Phys.*, 1955, **23**, 1841-1846.
47. P. O. Löwdin, *J. Chem. Phys.*, 1950, **18**, 365-375.
48. F. L. Hirshfeld, *Theor. Chim. Acta*, 1977, **44**, 129-138.
49. A. V. Marenich, S. V. Jerome, C. J. Cramer, D.G. Truhlar, *J. Chem. Theory Comput.*, 2012, **8**, 527-541.
50. R. F. W. Bader, *Chem. Rev.* 1991, **91**, 893– 928.
51. R. F. W. Bader, Atoms in Molecules: A Quantum Theory; International Series of Monographs on Chemistry 22; Oxford University Press: Oxford, U.K., **1990**.
52. C. F. Matta, N. Castillo, R. J. Boyd, *J. Phys. Chem. B* 2006, **110**, 563–578.
53. C. R. Wick, T. Clark, *J. Mol. Model.* 2018, **24**, 142.
54. P. S. V. Kumar, V. Raghavendra, V Subramanian, *J. Chem. Sci.* 2016, **128**, 1527–1536.
55. Keith, T. A. AIMAll, version 14.06.21; TK Gristmill Software: Overland Park, KS, **2014**.
56. G. A. Zhurko, Chemcraft 1.80 (build 523b) - graphical program for visualization of quantum chemistry computations, https://chemcraftprog.com.
57. C. B. Nielsen, J. M. Fraser, B. C. Schroeder, J. Du, A. J. P. White, W. Zhang and I. McCulloch, *Org. Lett.*, 2011, **13**, 2414-2417.
58. K. Morokuma, *J. Chem. Phys.*, 1971, **55**, 1236-1244.
59. G. te Velde, F. M. Bickelhaupt, E. J. Baerends, C. Fonseca Guerra, S. J. A. van Gisbergen, J. G. Snijders and T. Ziegler, *J. Comput. Chem.*, 2001, **22**, 931-967.
60. X. Guo, S. Wang, V. Enkelmann, M. Baumgarten and K. Müllen, *Org. Lett.*, 2011, **13**, 6062-6065.
61. H. Ueno, T. Nishihara, Y. Segawa and K. Itami, *Angew. Chem. Int. Ed.*, 2015, **54**, 3707-3711.
62. A. J. Stasyuk, O. A. Stasyuk, M. Solà and A. A. Voityuk, *Chem. Commun.*, 2019, **55**, 11195-11198.
63. A. J. Stasyuk, O. A. Stasyuk, M. Solà and A. A. Voityuk, *J. Phys. Chem. C*, 2019, **123**, 16525-16532.
64. A. J. Stasyuk, O. A. Stasyuk, M. Solà and A. A. Voityuk, *J. Phys. Chem. B*, 2020, **124**, 9095-9102.
65. A. J. Stasyuk, O. A. Stasyuk, S. Filippone, N. Martin, M. Solà and A. A. Voityuk, *Chem. Eur. J.*, 2018, **24**, 13020-13025.

66. A. J. Stasyuk, O. A. Stasyuk, M. Solà and A. A. Voityuk, *Phys. Chem. Chem. Phys.*, 2019, **21**, 25098-25107.
67. B. Mennucci, *Wiley Interdiscip. Rev. Comput. Mol. Sci.*, 2012, **2**, 386-404.
68. S.Grimme, *J. Chem. Phys.* 2013, **138**, 244104.
69. A. Chantzis, A. D. Laurent, C. Adamo, D. Jacquemin, *J. Chem. Theory Comput.* 2013, **9**, 4517– 4525.
70. L. Goerigk, S. Grimme, *J. Chem. Phys.* 2010, **132**, 184103.
71. Y. Jiang, P. Lv, J.-Q. Pan, Y. Li, H. Lin, X.-W. Zhang, J. Wang, Y.-Y. Liu, Q. Wei, G.-C. Xing, W.-Y. Lai, W. Huang, *Adv. Funct. Mater.* 2019, **29**, 1806719.
72. X.-C. Li, Y. Zhang, C.-Y. Wang, Y. Wan, W.-Y. Lai, H. Pang, W. Huang, *Chem. Sci.*, 2017, **8**, 2959-2965
73. X. Li, C. Wang, W. Song, C. Meng, C. Zuo, Y. Xue, W.-Y. Lai, W. Huang, *ChemPlusChem* 2019, **84**, 1623.
74. X.-C. Li, C.-Y. Wang, Y. Wan, W.-Y. Lai, L. Zhao, M.-F. Yin and W. Huang, *Chem. Commun.*, 2016, **52**, 2748-2751.
75. X.-C. Li, C.-Y. Wang, W.-Y. Lai and W. Huang, *J. Mat. Chem. C*, 2016, **4**, 10574-10587.
76. C.-F. Liu, X. Liu, W.-Y. Lai, W. Huang, *Chem. Rec.* 2019, **19**, 1571-1595.
77. H. Zhang, X. Liu, T.-T. Lu, P. Lv, W.-Y. Lai, *Chem. Eur. J.* 2019, **25**, 3909-3917.
78. J. Ulstrup and J. Jortner, *J. Chem. Phys.*, 1975, **63**, 4358-4368.
79. J. Jortner, *J. Chem. Phys.*, 1976, **64**, 4860-4867.